SUPPORTING INFORMATION

1,10-Phenanthrolines with tunable luminescence upon protonation: a spectroscopic and computational study

Andrea Listorti,[#] Alessandra Degli Esposti,[#] Ravuri S. K. Kishore,[§] Venkateshwarlu Kalsani,[§] Michael Schmittel,*[,§] Nicola Armaroli*[,#]

Center of Micro and Nanochemistry and Engineering, Organische Chemie I, Universität Siegen, Adolf-Reichwein-Str., D-57068 Siegen, Germany and Molecular Photoscience Group, Istituto per la Sintesi Organica e la Fotoreattività, Consiglio Nazionale delle Ricerche, Via Gobetti 101, 40129 Bologna, Italy

NMR characterization data sheets.

2-(3,5-Di-*tert*-butyl-4-methoxyphenyl)-9-(3-*tert*-butyl-4-methoxyphenyl)-[1,10]phenanthroline (**2**). M.p. 231-234 °C; ^{1}H NMR (400 MHz, $CDCl_3$) δ = 1.50 (s, 9 H, 3'-*t*-Bu), 1.60 (s, 18 H, 3'', 5''-*t*-Bu), 3.77 (s, 3 H, 4'-OMe), 3.96 (s, 3 H, 4''-OMe), 7.04 (d, ^{3}J = 8.6 Hz, 1 H, 5'-H), 7.75 (s, 2 H, 5,6-H), 8.08 (d, ^{3}J = 8.0 Hz, 1 H, 3-H), 8.09 (d, ^{3}J = 8.3 Hz, 1 H, 8-H), 8.12 (d, ^{4}J = 2.4 Hz, 1 H, 2'-H), 8.27 (d, ^{3}J = 8.0 Hz, 1 H, 4-H), 8.28 (d, ^{3}J = 8.3 Hz, 1 H, 7-H), 8.36 (s, 2 H, 2'', 6''-H), 8.58 (dd, ^{3}J = 8.6 Hz, ^{4}J = 2.4 Hz, 1 H, 6'-H) ppm. ^{13}C-NMR (100 MHz, $CDCl_3$) δ= 29.9, 32.2, 35.0, 36.0, 55.1, 64.4, 111.8, 119.5, 119.9, 125.4, 125.6, 125.7, 126.3 (2C), 127.3, 127.4, 131.6, 134.0, 136.7, 138.0, 143.9, 145.9 (3C), 157.0, 157.3, 159.9, 161.2 ppm; ESI-MS calcd for $C_{38}H_{45}N_2O_2$ [M+H$^+$]: *m/z* 561.77, found *m/z* (%) 561.6 (100), [M+H$^+$]; IR (KBr): ν 3458, 2958, 2868, 1602, 1588, 1541, 1486, 1463, 1425, 1407, 1392, 1360, 1314, 1236, 1180, 1143, 1116, 1093, 1030, 1010, 888, 850, 827, 817, 799, 739, 703, 634, 530; Anal. calcd**.** for $C_{38}H_{44}N_2O_2{\cdot}H_2O$: C, 78.86; H, 8.01; N, 4.84; Found: C, 79.01; H, 7.97; N, 4.63.

2,9-Bis-(2,4-dimethoxyphenyl)-[1,10]phenanthroline (**3**). M.p. 134 °C; ^{1}H NMR ($CDCl_3$, 400 MHz): δ 3.90 (s, 12 H, -OMe), 6.60 (d, ^{4}J = 2.2 Hz, 2 H, 3', 3''-H), 6.74 (dd, ^{3}J = 8.6 Hz, ^{4}J = 2.2 Hz, 2 H, 5', 5''-H), 7.74 (s, 2 H, 5, 6-H), 8.19 (d, ^{3}J = 8.6 Hz, 2 H, 3, 8-H), 8.25 (d, ^{3}J = 8.6 Hz, 2 H, 4, 7-H), 8.38 (d, ^{3}J = 8.6 Hz, 2 H, 6', 6''-H) ppm; ^{13}C NMR ($CDCl_3$, 100 MHz): δ = 55.5, 55.8, 99.0, 105.5, 122.6, 124.4, 125.5, 127.1, 133.4, 135.3, 145.8, 155.8, 158.8, 161.7 ppm; ESI MS: calcd. for $C_{28}H_{25}N_2O_4$ [M+H$^+$]: *m/z* 453.5, found: *m/z* (%) 454.2 (100); IR (KBr): ν 3358, 2996, 2935, 1612, 1581, 1488, 1463, 1414, 1279, 1207, 1159, 1134, 1028, 937, 857, 828, 794, 748, 635; Anal. Calcd. for $C_{28}H_{24}N_2O_4{\cdot}H_2O$: C, 71.47; H, 5.57; N, 5.95. Found: C, 71.76; H, 5.56; N, 6.00.

2-(3-*tert*-Butyl-4-methoxyphenyl)-9-(2,4,6-trimethylphenyl)-[1,10]phenanthroline (**6**). M.p. 156-158 °C; ^{1}H NMR (400 MHz, $CDCl_3$): δ = 1.45 (s, 9 H, *t*-Bu), 2.25 (s, 6 H, 2'', 6''-Me), 2.37 (s, 3 H, 4''-Me), 3.89 (s, 3H, -OC$\underline{H}_3$), 6.98 (d, ^{3}J = 8.3 Hz, 1 H, 5'-H), 6.99 (s, 2 H, 3'', 5''-H), 7.60 (d, ^{3}J = 8.0 Hz, 1 H, 8-H), 7.78 (d, ^{3}J = 8.6 Hz, 1 H, 6-H), 7.80 (d, ^{3}J = 8.6 Hz, 1 H, 5-H), 8.04 (d, ^{3}J = 8.3 Hz, 1 H, 3-H), 8.06 (dd, ^{3}J = 8.6 Hz, ^{4}J = 2.4 Hz, 1 H, 6'-H) 8.26 (d, ^{3}J = 8.3 Hz, 1 H, 4-H), 8.27 (d, ^{3}J = 8.0 Hz, 1

H, 7-H), 8.31 (d, ^4J = 2.4 Hz, 1 H, 2'-H) ppm;^{13}C-NMR (100 MHz, $CDCl_3$): δ= 20.9, 21.2, 29.6, 35.0, 55.1, 111.5, 120.0, 125.0, 125.5, 126.0, 126.5, 126.8, 127.1(2C), 128.6, 131.8, 135.6, 136.4, 136.5, 137.4, 137.8, 138.4, 145.9, 146.1, 157.5, 159.5, 159.8 ppm; ESI-MS calcd. for $C_{32}H_{33}N_2O$ [M+H$^+$]: *m/z* 461.61, found m/z (%) 461.6 (100), [M+H$^+$]; IR (KBr): ν 3417, 2956, 2867, 2562, 2247, 1947, 1601, 1587, 1486, 1462, 1389, 1358, 1314, 1276, 1239, 1094, 1029, 855, 819, 801, 734, 702, 632; Anal calcd. for $C_{32}H_{32}N_2O{\cdot}H_2O$: C, 80.30; H, 7.16; N, 5.85; Found: C, 80.32; H, 7.44; N, 5.30.

2-(3-*tert*-Butyl-4-methoxyphenyl)-[1,10]phenanthroline (**8**). Mp**:** 73-75 °C. ^{1}H NMR (400 MHz, $CDCl_3$) δ= 1.49 (s, 9 H, *t*-Bu), 3.93 (s, 3 H, O-CH_3), 7.04 (d, *J* = 8.5 Hz, 1 H, 5′-H), 7.63 (dd, *J* = 8.0, 4.3 Hz, 1 H, 8-H), 7.74 (d, *J* = 8.7 Hz, 1 H, 6-H), 7.80 (d, *J* = 8.7 Hz, 1 H, 5-H), 8.06 (d, *J* = 8.4 Hz, 1 H, 3-H), 8.19 (d, *J* = 2.3 Hz, 1 H, 2′-H), 8.28 (m, 3 H, 6′-, 4-, 7-H), 9.23 (dd, *J* = 4.3, 1.6 Hz, 1 H, 9-H);^{13}C-NMR (100 MHz, $CDCl_3$) δ= 29.7, 35.0, 55.2, 111.8, 120.4, 122.7, 125.6, 126.2, 126.5, 127.0, 127.3, 129.0, 131.7, 136.2, 136.5, 138.2, 145.9, 146.2, 150.1, 158.0, 159.9; ESI-MS calcd for $C_{23}H_{23}N_2O$ [M+H$^+$]: *m/z* 343.44, found *m/z* (%) 343.5 (100), [M+H$^+$]; IR (KBr): ν 3479, 2956, 1620, 1549, 1490, 1409, 1390, 1275, 1238, 1202, 1145, 1093, 1028, 849, 812, 777, 743, 704, 671, 627, 533, 516; Anal. calcd**.** for $C_{23}H_{22}N_2O{\cdot}¼H_2O$: C, 79.62; H, 6.54; N, 8.07; Found C, 79.52; H, 6.78; N, 7.84.

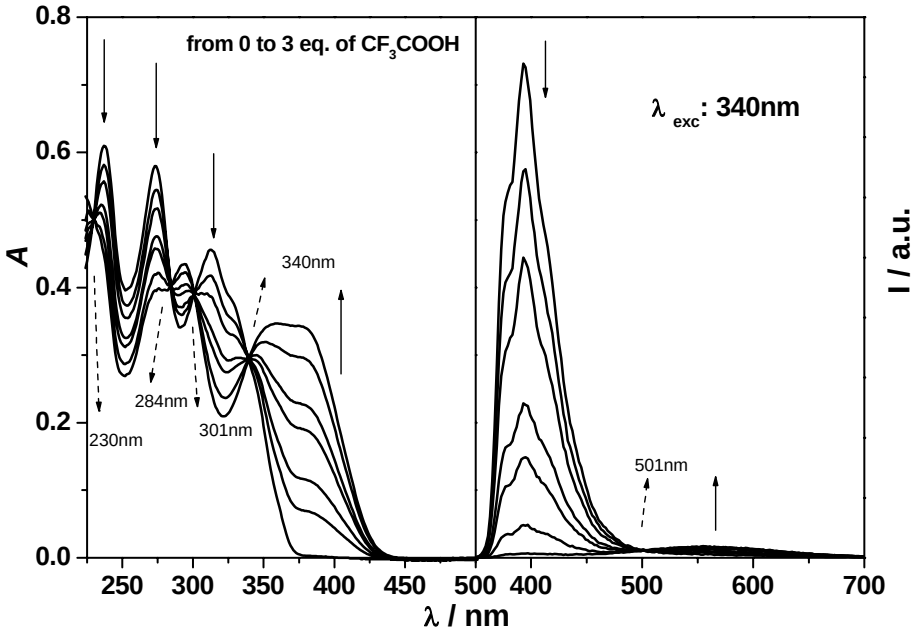

Figure S1. Changes of the absorption (left) and fluorescence spectra (right, λ_{exc} = 340 nm) of a 5 x 10^{-6} M solution of **1** in CH_2Cl_2 upon addition of increasing amounts of trifluoroacetic acid (from 0 to 1.5 x 10^{-5} M). Dashed arrows indicate isosbestic and isoemissive points.

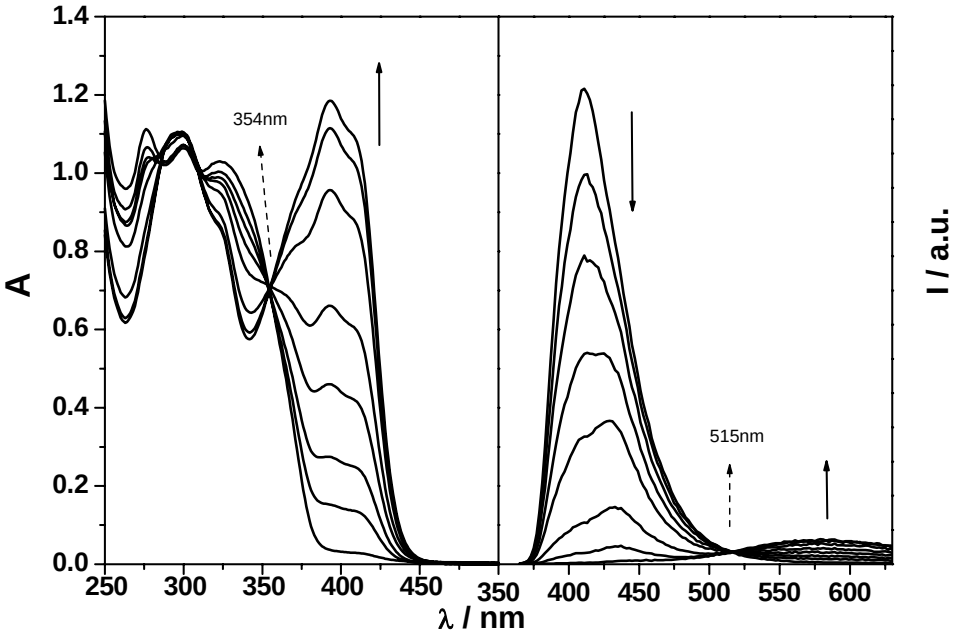

Figure S2. Changes of the absorption (left) and fluorescence spectra (right, λ_{exc} = 354 nm) of a 5 x 10^{-6} M solution of **3** in CH_2Cl_2 upon addition of increasing amounts of trifluoroacetic acid (from 0 to 1.5 x 10^{-5} M). Dashed arrows indicate isosbestic and isoemissive points.

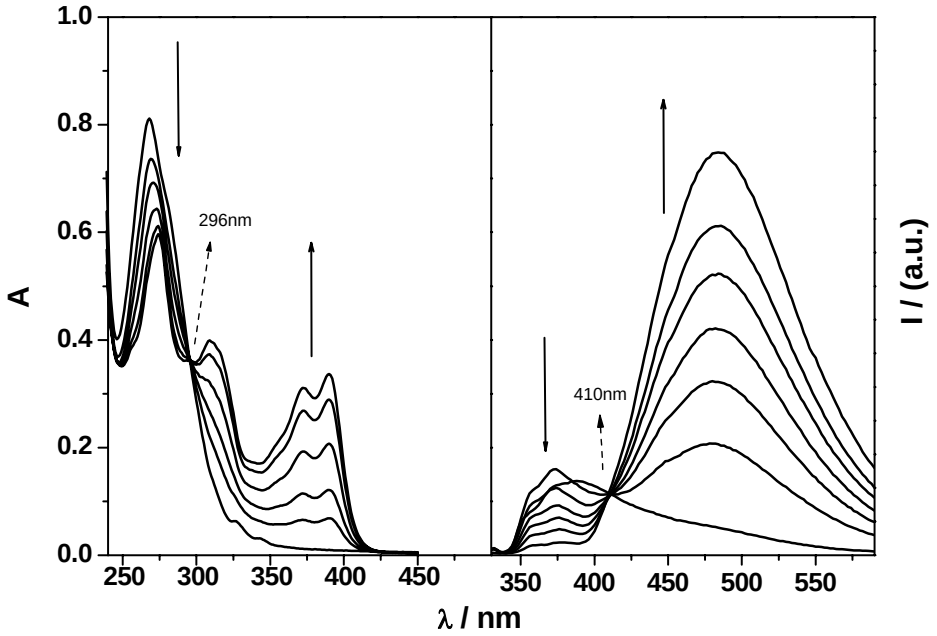

Figure S3. Changes of the absorption (left) and fluorescence spectra (right, λ_{exc} = 296 nm) of a 5 x 10^{-6} M solution of **4** in CH_2Cl_2 upon addition of increasing amounts of trifluoroacetic acid (from 0 to 5 x 10^{-6} M). Dashed arrows indicate isosbestic and isoemissive points.

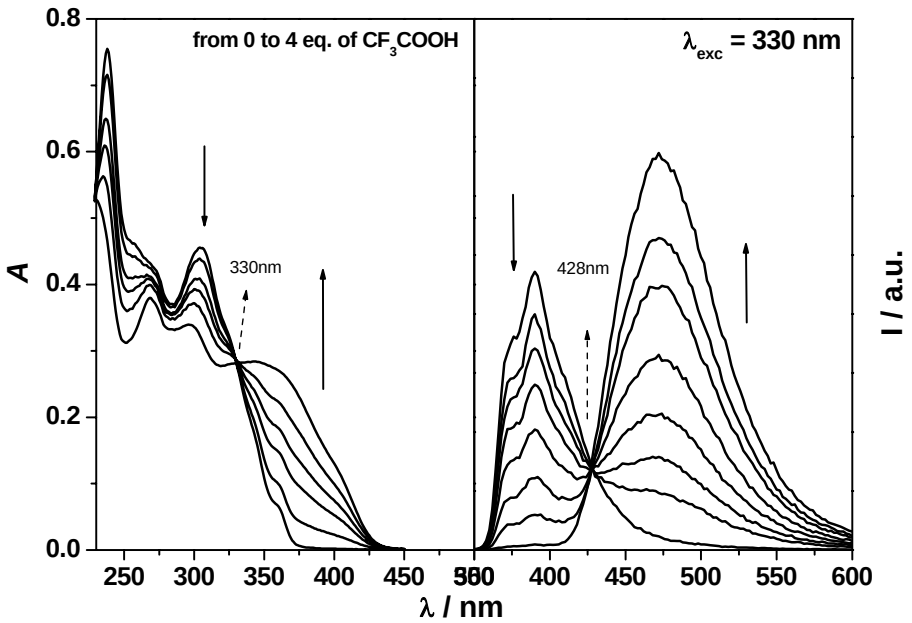

Figure S4. Changes of the absorption (left) and fluorescence spectra (right, λ_{exc} = 330 nm) of a 5 x 10^{-6} M solution of **7** in CH_2Cl_2 upon addition of increasing amounts of trifluoroacetic acid (from 0 to 2.0 x 10^{-5} M). Dashed arrows indicate isosbestic and isoemissive points.

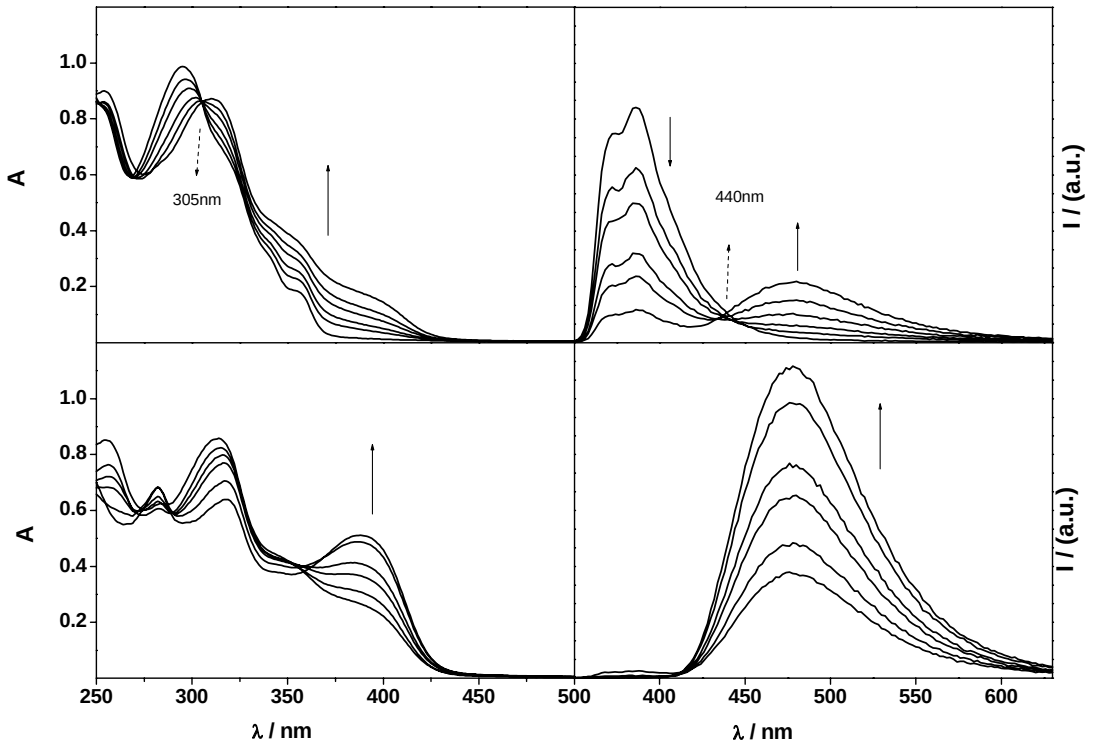

Figure S5. Top: changes of the absorption (left) and fluorescence spectra (right, λ_{exc} = 313– nm) of a 5 x 10^{-6} M solution of **9** in CH_2Cl_2 upon addition of increasing amounts of trifluoroacetic acid (from 0 to 3.0 x 10^{-6} M). Bottom: Further changes in the absorption and fluorescence spectra (λ_{exc} = 374 nm) upon addition of acid up to 2.5 x 10-3 M (500 equivalents). Dashed arrows indicate isosbestic and isoemissive points.

Table S1. Luminescence properties of **1-9** in CH_3CN vs CH_2Cl_2

	CH_3CN			CH_2Cl_2		
	λ_{max}[a] (nm)	Φ_{em}[b]	τ[c] (ns)	λ_{max}[a] (nm)	Φ_{em}[b]	τ[c] (ns)
1	391	0.075	1.6	393	0.12	1.8
2	405	0.13	2.1	404	0.26	1.8
3	411	0.30	1.7	408	0.33	1.6
4	407	[d]	[d]	394	0.007	< 0.1[e]
5	[d]	[d]	[d]	374	0.0005	< 0.1[e]
6	399	0.18	1.8	398	0.12	1.5
7	387	0.03	0.8	391	0.08	1.0
8	399	0.2	2.0	398	0.24	2.0
9	385	0.062	1.1	388	0.11	1.2

[a]Emission maxima from spectra corrected for the instrumental response. [b]Fluorescence quantum yields in air-equilibrated solutions. [c]Excited state singlet lifetimes in air-equilibrated solutions (λ_{exc} = 278 nm). [d]Not detected..[e] Ultrashort and below instrumental resolution.

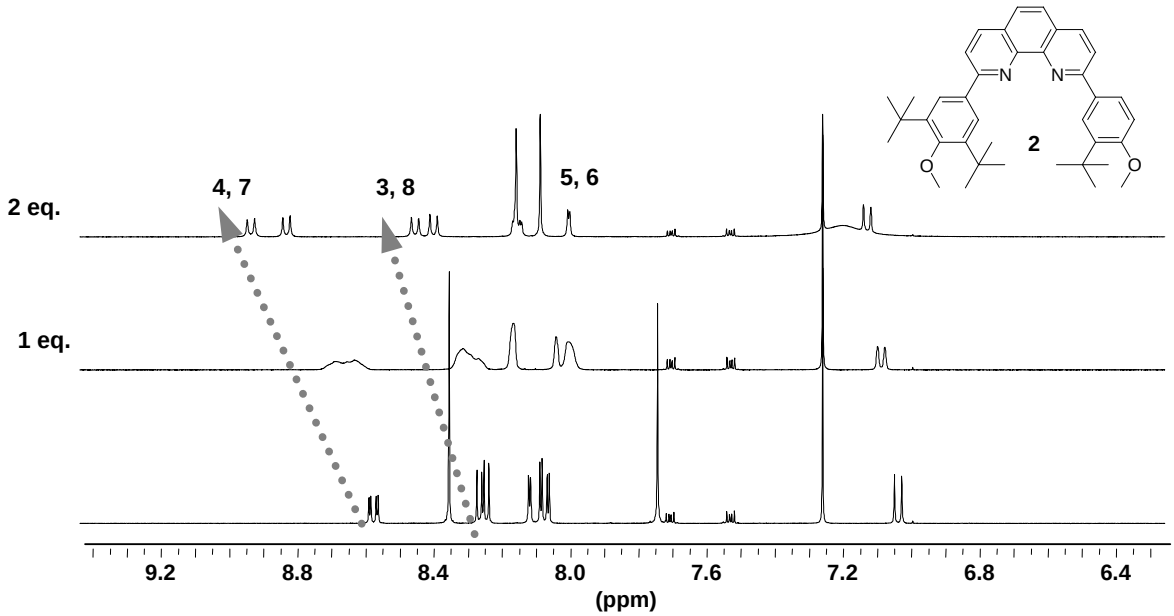

Figure S6. Changes in the ^{1}H NMR of phenanthroline 2 upon addition of 2 equivalents of TFA in $CDCl_3$.

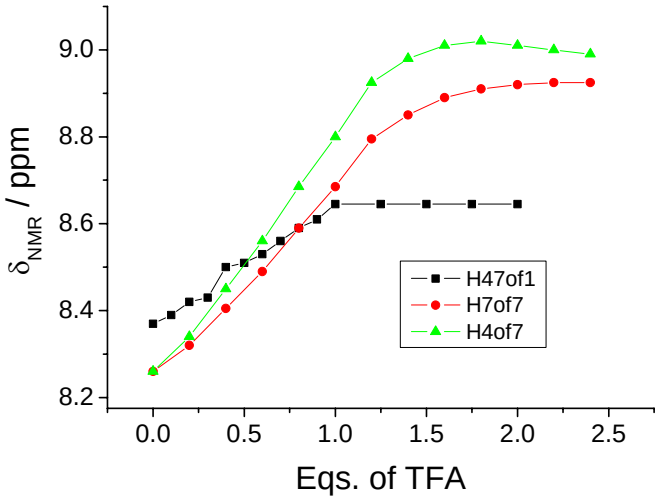

Figure S7: ^{1}H NMR shifts of protons 7-H and 4-H of phenanthrolines **1** and **7** (0.05 M solution in $CDCl_3$) in the their titrations against TFA.

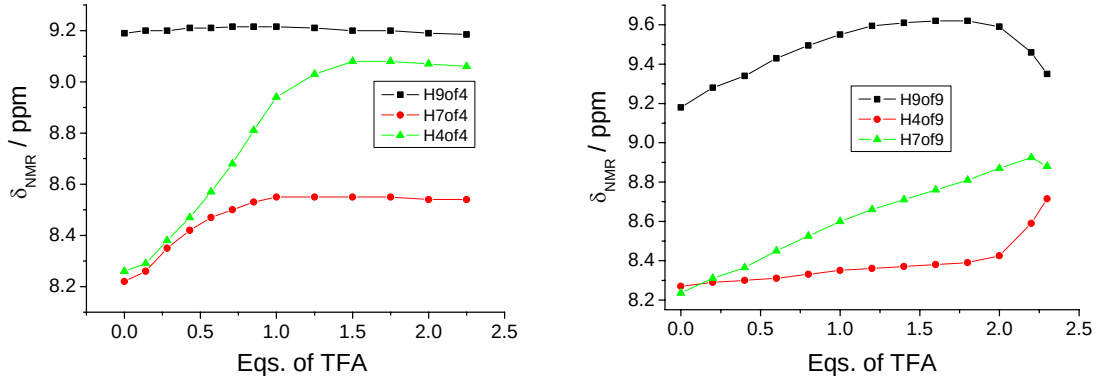

Figure S8: ^{1}H NMR shifts of protons 9-H, 7-H and 4-H of phenanthrolines **4** (left) and **9** (right) (0.05 M solution in $CDCl_3$) in the their titrations against TFA.

Details on TD-DFT and TD-HF calculations of 1-9 and their protonated forms.

· The calculations were performed using:

Gaussian 03, Revision D.02,

M. J. Frisch, G. W. Trucks, H. B. Schlegel, G. E. Scuseria, M. A. Robb, J. R. Cheeseman, J. A. Montgomery, Jr., T. Vreven, K. N. Kudin, J. C. Burant, J. M. Millam, S. S. Iyengar, J. Tomasi, V. Barone, B. Mennucci, M. Cossi, G. Scalmani, N. Rega, G. A. Petersson, H. Nakatsuji, M. Hada, M. Ehara, K. Toyota, R. Fukuda, J. Hasegawa, M. Ishida, T. Nakajima, Y. Honda, O. Kitao, H. Nakai, M. Klene, X. Li, J. E. Knox, H. P. Hratchian, J. B. Cross, V. Bakken, C. Adamo, J. Jaramillo, R. Gomperts, R. E. Stratmann, O. Yazyev, A. J. Austin, R. Cammi, C. Pomelli, J. W. Ochterski, P. Y. Ayala, K. Morokuma, G. A. Voth, P. Salvador, J. J. Dannenberg, V. G. Zakrzewski, S. Dapprich, A. D. Daniels, M. C. Strain, O. Farkas, D. K. Malick, A. D. Rabuck, K. Raghavachari, J. B. Foresman, J. V. Ortiz, Q. Cui, A. G. Baboul, S. Clifford, J. Cioslowski, B. B. Stefanov, G. Liu, A. Liashenko, P. Piskorz, I. Komaromi, R. L. Martin, D. J. Fox, T. Keith, M. A. Al-Laham, C. Y. Peng, A. Nanayakkara, M. Challacombe, P. M. W. Gill, B. Johnson, W. Chen, M. W. Wong, C. Gonzalez, and J. A. Pople, Gaussian, Inc., Wallingford CT, 2004.

· The methods used, i.e. TD-B3LYP/6-31G*, TD-BHandLYP/6-31G*, and TD-HF/6-31G*, are herewith referred to as **I**, **II**, and **III**, respectively.

· Wavelengths (λ) in nm and oscillator strenghts ($f_{osc.}$) of transitions to the singlet first and second excited states ($^1\mathbf{S}_0 \rightarrow {}^1\mathbf{S}_n$, n=1, and 2) are reported.

· Unless differently specified, in the following we refer to the planar geometries.

· Molecular drawing perfomed using MOLDEN: G.Schaftenaar and J.H. Noordik, J. Comput.-Aided Mol. Design, **2000**, *14*, 123.

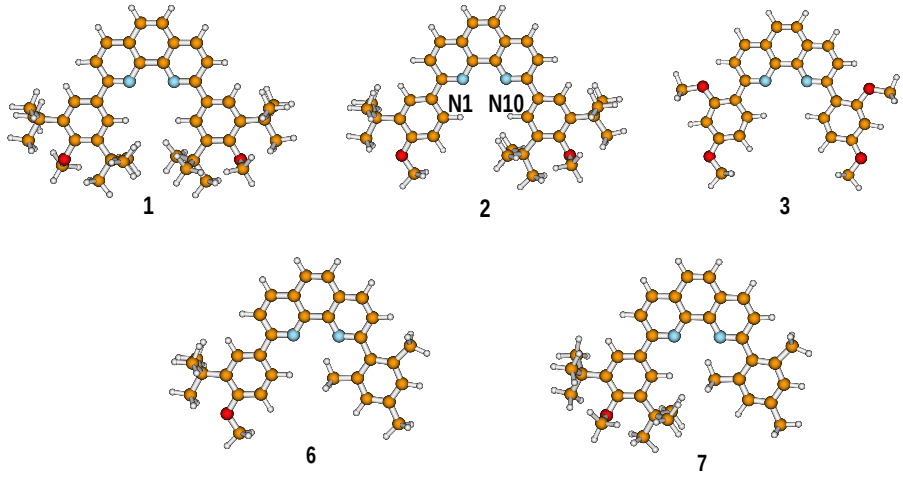

Table S2: **1**, **2**, **3**, **6**, and **7**

	$^1\mathbf{S}_0 \rightarrow {}^1\mathbf{S}_n$	**1**		**2**		**3**		**6**		**7**	
	n.	λ	$f_{osc.}$	λ	$f_{osc.}$	λ	$f_{osc.}$	λ	$f_{osc.}$	λ	$f_{osc.}$
I	1	358	0.4574	367	0.4428	372	0.4722	369	0.4195	360	0.4185
	2	342	0.0199	350	0.0114	347	0.0461	350	0.0224	346	0.0004
II	1	314	0.6051	316	0.6301	322	0.6283	319	0.5949	315	0.5644
	2	301	0.0456	303	0.0400	303	0.1199	303	0.0551	301	0.0599
III	1	293	0.4477	293	0.4667	295	0.4957	294	0.4554	293	0.4353
	2	270	0.1002	269	0.0927	272	0.2148	270	0.1216	269	0.1191

Table S3: $\mathbf{1{\cdot}H^+}$, $\mathbf{2{\cdot}H^+_{N1}}$, $\mathbf{2{\cdot}H^+_{N10}}$, $\mathbf{3{\cdot}H^+}$

	$^1\mathbf{S}_0 \rightarrow {}^1\mathbf{S}_n$	$\mathbf{1{\cdot}H^+}$		$\mathbf{2{\cdot}H^+_{N1}}$		$\mathbf{2{\cdot}H^+_{N10}}$		$\mathbf{3{\cdot}H^+}$	
	n.	λ	$f_{osc.}$	λ	$f_{osc.}$	λ	$f_{osc.}$	λ	$f_{osc.}$
I	1	541	0.0088	526	0.0122	629	0.0093	578	0.0093
	2	488	0.0032	486	0.0023	444	0.1409	441	0.0011
II	1	383	0.0360	379	0.1117	410	0.0212	396	0.0391
	2	345	0.6854	354	0.6035	345	0.8083	353	0.7491
III	1	308	0.5844	313	0.6670	308	0.4727	343	0.8861
	2	291	0.1182	289	0.0872	294	0.2459	310	0.7104

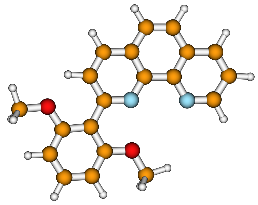

4^a

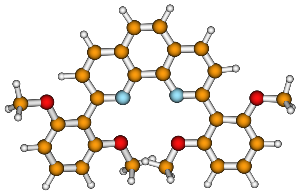

5^a

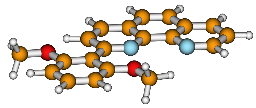

4^b

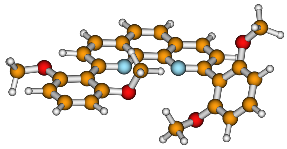

5^b

Table S4: **4** and **5**.

	$^1S_0 \rightarrow ^1S_n$	**4**^{a}		**4**^{b}		**5**^{a}		**5**^{b}	
	n.	λ	$f_{osc.}$	λ	$f_{osc.}$	λ	$f_{osc.}$	λ	$f_{osc.}$
I	1	325	0.1727	351	0.0007	323	0.2105	353	0.0020
	2	322	0.0114	336	0.3810	320	0.0616	340	0.3967

^{a} Ground state geometry.

^{b} Planar geometry (only one aryl can lie on the plane of 1,10-phenanthroline in case of **5**).

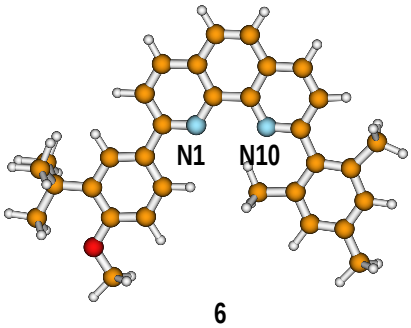

6

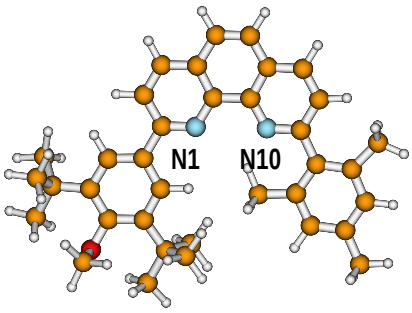

7

Table S5: Protonated forms of **6**, and **7**.

	$^1\mathbf{S}_0 \rightarrow {}^1\mathbf{S}_n$	$\mathbf{6}\cdot\mathbf{H}^+_{N1}$		$\mathbf{6}\cdot\mathbf{H}^+_{N10}$		$\mathbf{6}\cdot\mathbf{H}^{2+}_2$		$\mathbf{7}\cdot\mathbf{H}^+_{N1}$		$\mathbf{7}\cdot\mathbf{H}^+_{N10}$		$\mathbf{7}\cdot\mathbf{H}^{2+}_2$	
	n.	λ	$f_{osc.}$	λ	$f_{osc.}$	λ	$f_{osc.}$	λ	$f_{osc.}$	λ	$f_{osc.}$	λ	$f_{osc.}$
I	1	502	0.0137	616	0.0131	560	0.0703	511	0.0110	530	0.0135	511	0.0158
	2	452	0.0102	438	0.1606	464	0.2266	462	0.0033	480	0.0016	493	0.0965
II	1	376	0.1755	405	0.0316	413	0.5310	378	0.0451	378	0.0460	394	0.6288
	2	352	0.5476	340	0.7141	359	0.4510	345	0.6841	337	0.6270	375	0.0620
III	1	313	0.6867	307	0.4514	342	0.8659	309	0.5905	305	0.5268	335	0.8398
	2	288	0.0738	292	0.2498	307	0.6538	290	0.0979	290	0.1478	306	0.5746

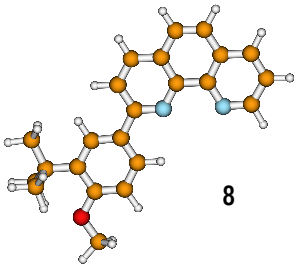

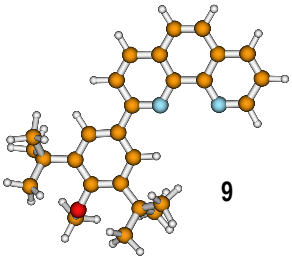

Table S6: **8**, **9**.

	I				**II**				**III**			
$^1\mathbf{S}_0 \rightarrow {}^1\mathbf{S}_n$	**8**		**9**		**8**		**9**		**8**		**9**	
n.	λ	$f_{osc.}$	λ	$f_{osc.}$	λ	$f_{osc.}$	λ	$f_{osc.}$	λ	$f_{osc.}$	λ	$f_{osc.}$
1	345	0.2483	333	0.2361	302	0.5412	297	0.4579	281	0.4767	278	0.4135
2	341	0.3010	328	0.2868	291	0.1579	288	0.1661	262	0.0093	261	0.0139

Table S7: Protonated forms of **8**, and **9**.

	$^1\mathbf{S}_0 \rightarrow {}^1\mathbf{S}_n$	$\mathbf{8}\cdot\mathbf{H}^+_{N1}$		$\mathbf{8}\cdot\mathbf{H}^+_{N10}$		$\mathbf{8}\cdot\mathbf{H}^{2+}_2$		$\mathbf{9}\cdot\mathbf{H}^+_{N1}$		$\mathbf{9}\cdot\mathbf{H}^+_{N10}$		$\mathbf{9}\cdot\mathbf{H}^{2+}_2$	
	n.	λ	$f_{osc.}$	λ	$f_{osc.}$	λ	$f_{osc.}$	λ	$f_{osc.}$	λ	$f_{osc.}$	λ	$f_{osc.}$
II	1	360	0.7048	446	0.0105	446	0.2545	349	0.6719	417	0.0114	422	0.2509
	2	305	0.0202	347	0.4587	371	0.4493	322	0.0279	351	0.0010	410	0.0599
III	1	313	0.8041	315	0.0205	349	0.8269	307	0.7448	308	0.0240	337	0.7792
	2	273	0.0068	292	0.3992	293	0.2942	274	0.0028	287	0.2478	301	0.0361

A brief comment about the results calculated by different methods.

The TD-B3LYP method adequately describes the energetic and intensity trends shown by **1**, **2**, **3**, **6**, and **7** (Table S2) and, with less accuracy, the protonated forms of the first three compounds (Table S3). Neither of TDDFT methods employed are able to reproduce the increasing intensity trend shown by the emissions of **1**·H^+, **2**·H^+, and **3**·H^+, whereas TDHF succeeds, though it largely overestimates them. In the case of the asymmetric compounds **6**·H^+ and **7**·H^+ (Table S5) only TDHF is able to properly account for the π-π^* excitation which gives rise to their intense first excited state transitions. In the case of **8** and **9** (Table S6) TD-B3LYP also fails in properly resolving the calculated near degeneracy of the first two excited states, whereas TD-BHandLYP succeeds and shows the correct trend of the calculated intensities, i.e. that of **8** larger than that of **9**. Moreover, it calculates oscillator strengths for **8**·H^+_{N1} and **9**·H^+_{N1} much larger than those of their basic forms, while much weaker transition intensities are obtained for the other protonated forms, in agreement also with the TDHF results. The oscillator strengths of **8**·H^{2+}_2 and **9**·H^{2+}_2 calculated by TD-BHandLYP (Table S7) are much weaker than those obtained by TDHF which, similarly to the asymmetric **6**·H^+ and **7**·H^+ compounds, shows a different energy ordering of their highest occupied MOs. TD-B3LYP calculates (Table S4) very close transition energies for **4** and **5**, and shows the presence of a low lying σ excited state, which is tuned by changes of the molecular geometry.